Electrophysiological Study with Oxonol VI of Passive NO_3^- Transport by Isolated Plant Root Plasma Membrane

P. Pouliquin, J.-P. Grouzis, and R. Gibrat

Biochimie et Physiologie Moléculaire des Plantes, CNRS (URA 2133)/INRA/ENSA-M, Montpellier, France

ABSTRACT In contrast to animal cells, plant cells contain ~5–50 mM nitrate in cytosol and vacuole. The lack of specific spectroscopic probes, or suitable isotopes, impedes in vitro studies of NO_3^- transport. Reconstitution of root cell plasma membrane (PM) proteins in mixed soybean lipid:egg phosphatidylcholine allowed for the generation of large K^+-valinomycin diffusion potentials (E_m), monitored with the oxonol VI dye. Nevertheless, E_m was restricted to ~130 mV by capacitor properties of biological membranes. This caused an increasing discrepancy at higher K^+-Nernst potentials used for calibration. Therefore, E_m was determined directly from the fluorescence of the dye free in buffer, bound at zero E_m, and bound upon E_m generation. Then, an electrophysiological analysis of the NO_3^--dependent dissipation rate of E_m gave the net passive flux (J_N) and the permeability coefficient to NO_3^- (P_N). The plant root cell PM exhibited a strikingly large P_N (higher than 10^{-9} m s^{-1}) at high E_m (90–100 mV) and pH 6.5. At low E_m (50–60 mV) and pH 7.4, P_N decreased by 70-fold and became similar to that of the lipid bilayer. This agreed with the previous observation that 15 mM NO_3^- short-circuits the plant root PM H^+-ATPase at its optimal pH of 6.5.

INTRODUCTION

Plasma membrane (PM) H^+-ATPase of plant, algae, and fungus generates membrane potentials (E_m) up to 250 mV (Gradmann et al., 1978; Sanders and Slayman, 1989). We showed elsewhere (Grouzis et al., 1997) that inside-out PM vesicles from root cells, double-labeled with fluorescent probes for pH and E_m, cannot be acidified in the absence of permeant ionic species to electrically compensate pumped H^+; as expected, the pump stalls on the high, positive-inside E_m it creates. Short-circuiting the H^+-ATPase at pH 6.5, the acidic optimum of plant PM H^+ pumps, triggers its maximal H^+-pumping rate; this can be achieved by adding the K^+ ionophore valinomycin to vesicles loaded with 100 mM K^+ or, alternatively, by adding only 15 mM NO_3^- to the outside of non-K^+-loaded vesicles. This NO_3^- short-circuiting reveals a concurrent (electrically coupled) transport of H^+ and NO_3^-. It is saturable, inhibitable, and thermolabile and not observable, by contrast, with liposomes containing only the purified H^+-ATPase. In this way, the root cell PM appears more conductive to NO_3^- than to Cl^- or even to K^+, due to a protein-mediated passive pathway (i.e., driven by the transmembrane ion electrochemical gradient).

Anion transport at the animal cell PM is mainly attributable to Cl^- and HCO_3^- (Stein, 1986). Plant cells, which ensure the major N input in terrestrial trophic chains, contain usually ~5 and 50 mM in cytosol and vacuole, respectively (Zhen et al., 1992). Channels confer highly conductive passive pathways to anions in leaf guard cell PM, and a permeability coefficient 4- to 10-fold higher for NO_3^- (P_N) than for Cl^- (Schmidt and Schroeder, 1994; Hedrich and Marten, 1993). Although large passive NO_3^- efflux from root cells can be transiently observed (for example, Delhon et al., 1995), no channels for passive NO_3^- efflux have been found to date in mature cortical root cells, despite attempts (Ryan et al., 1997). This prompted us to examine in vitro the passive NO_3^- transport and permeability coefficient of plant root cell PM.

Isolated vesicles are suitable to control ion concentrations across the membrane and to determine net ion fluxes and permeability coefficients, by measuring filling or emptying kinetics (Venema et al., 1993). Furthermore, inside-out PM vesicles make transport sites of passive efflux systems accessible to the external medium. Unfortunately, the lack of specific or suitable spectroscopic probes and isotopes impedes in vitro studies. We have shown that NO_3^- strongly increases the dissipation rate of K^+-valinomycin diffusion E_m across PM vesicles, qualitatively monitored with the oxonol VI dye (Grouzis et al., 1997). This offered a more direct access to passive NO_3^- transport by PM proteins, compared with NO_3^--coupled H^+-pumping rate evoked above.

As plant cells are strongly polarized, the aim of the present work was to generate large K^+-valinomycin diffusion E_m. This revealed an inconsistency between the response of oxonol VI and theoretical (K^+-Nernst) E_m higher than 70 mV. The plot of oxonol response versus Nernst potential, which is classically used to calibrate E_m dyes, deviated increasingly from linearity due to capacitor properties of biological membranes (Apell and Bersch, 1987). The lipophilic anion oxonol VI, the most permeant cyanine dye, is expected to distribute freely across the membrane at thermodynamic equilibrium with E_m (Bashford et al., 1979; Clarke and Apell, 1989). We took advantage of this prop-

Received for publication 8 May 1998 and in final form 6 October 1998.

Address reprint requests to Dr. Rémy Gibrat, Biochimie et Physiologie Moléculaire des Plantes, ENSA-M/INRA/CNRS (URA 2133), F-34060 Montpellier Cedex 1, France. Tel.: (33) 4 99 61 23 68; Fax: (33) 4 67 52 57 37; E-mail: gibrat@ensam.inra.fr.

P. Pouliquin's present address: University of Ulm, Department of Applied Physiology, Germany.

0006-3495/99/01/360/14 $2.00

erty to determine E_m directly from the fluorescence of oxonol VI. Then, the electrophysiological analysis of the NO_3^--dependent E_m dissipation rate allowed the demonstration that the root cell PM exhibits, like that of leaf guard cells, a strikingly large permeability coefficient for NO_3^- (higher than 10^{-9} m s^{-1}). The corresponding conductive pathway appeared voltage dependent and detectable only at the acidic optimal pH of 6.5 of plant PM H^+-ATPase.

MATERIALS AND METHODS

Experimental materials

Corn seeds (*Zea mays* L., var Mona) were grown as described previously (Simon-Plas et al., 1991). Microsomes were prepared according to De Michelis and Spanswick (1986). Plasma membrane was further purified as described elsewhere (Galtier et al., 1988).

Protein reconstitution procedure

The PM protein moiety was reconstituted by rapid elimination of the detergent DOC in a Sephadex G-50 mini-column, at a lipid-to-protein ratio of 15 (w/w), according to Grouzis et al. (1997). Control liposomes of mixed soybean phospholipid:egg PC (8:2, w/w; soybean L-α-phosphatidylcholine, type II-S, and egg phosphatidylcholine, type XVI-E, Sigma Aldrich Chimie, France) were prepared in the same way. Otherwise stated, reconstitution was performed in a medium containing K_2SO_4 (0–50 mM, as indicated in text and legends), 0.1 M HEPES-Li (pH 7.4), 50 mM Li_2SO_4, and 20% (v/v) glycerol. As detailed elsewhere (Grouzis et al., 1997), this reconstitution procedure gave a homogeneous population of highly tight vesicles containing unidirectionally (inside-out) reinserted H^+-ATPase molecules with the same hydrolytic activity as the total one in native membrane (i.e., corresponding to the sum of the so-called basal plus latent activities, measured on a detergent-permeabilized mixture of native inside-out plus right-side-out vesicles). The H^+-ATPase in reconstituted PM vesicles remains short-circuited by NO_3^- and the NO_3^--coupled H^+ pumping exhibits similar K_m for NO_3^- as in native vesicles.

Encapsulation of pyranine in membrane vesicles

To encapsulate pyranine (8-hydroxy-1,3,6-pyrene-trisulfonic acid) into membrane vesicles, reconstitution was performed in the presence of 0.5 mM pyranine. Nonencapsulated probe was removed by gel filtration on a Sephadex G-50 mini-column. Pyranine was also encapsulated into sonicated and freeze-thawed liposomes. Eighty milligrams ml^{-1} phospholipids were dispersed in 0.1 M HEPES-Li (pH 7.4), 50 mM Li_2SO_4, 10 mM $CaSO_4$, and 0.5 mM pyranine, by vigorous mixing on a vortex mixer in the presence of glass beads for 15 min under argon. This suspension was sonicated for 20 min under argon in a Bransonic bath sonicator until clarification. Freeze-thawed liposomes were obtained from sonicated liposomes after four freeze-thaw (liquid nitrogen/ice) cycles. After 10-fold dilution in the same medium without $CaSO_4$, the suspension was passed through a Sephadex G-50 mini-column to remove nonencapsulated pyranine.

Determination of vesicles size

Two methods were used to determine vesicles size. It was estimated first from the fluorescence of entrapped pyranine recorded at 511 nm after excitation at 421 nm. The fluorescence decrease of the dye in the presence of the quencher DPX (*p*-xylene-bis-pyridinium bromide) indicated that more than 90% of the dye was entrapped. The specific internal volume V_1 (in 1 per mol of phospholipid) was given by

$$V_1 = C_a/(C_1\, Lip),$$

in which *Lip* is the molar concentration of phospholipids in the assay cuvette, C_1 the concentration of entrapped pyranine in the lumen (0.5 mM), and C_a the macroscopic concentration of pyranine in the assay cuvette, deduced from comparison of the fluorescence intensity of the sample and a calibration curve with bulk pyranine (in the absence of vesicles). Denoting s the molecular area of the phospholipids (75 $Å^2$, according to Gibrat and Grignon, 1983), A the vesicle mean area (in $Å^2$, corresponding to $2A$ of phospholipidic area), and N the Avogadro's number, R_v, the mean internal radius of the vesicles (in Å), is given by

$$R_v = 3V_1/2A = 6V_1/N\mathrm{s} = 133V_1$$

The second method to estimate vesicle size used gel filtration chromatography (Reynolds et al., 1983; Ollivon et al., 1986). A column (60 × 0.9 cm) was poured with Sephacryl S-1000SF at a flow rate of 0.25 ml/min. Vesicle samples were chromatographed on columns presaturated with three column volumes containing 0.25 mg ml^{-1} sonicated soybean lipids in 0.1 M HEPES-Li (pH 7.4), 50 mM Li_2SO_4. A 500-μl aliquot of sample (1 mg of lipid) was layered on the top of the column and eluted at the same flow rate in elution buffer containing 0.1 M HEPES-Li (pH 7.4), 50 mM Li_2SO_4. The total volume (V_t) and the void volume (V_0) of the column were determined from the elution of a peptide (Gly-Tyr, molecular weight 238.2) and multilamellar vesicle (MLV) lipid or latex beads (diameter, 5.7 μm), respectively. For calibration of the column with latex beads (diameters, 97 ± 13 and 302 ± 6 nm), the column was equilibrated and eluted with elution buffer containing 3 mM sodium dodecyl sulfate (SDS) to prevent aggregation of the latex beads (Reynolds et al., 1983), and Li_2SO_4 was replaced by NaCl in elution buffer to avoid precipitation. The effluent was monitored by optical density at 280 nm. Vesicle radius was estimated by the procedure of Ackers (1967). A partition coefficient, designated K_{av}, is given by

$$K_{av} = (V_e - V_0)/(V_t - V_0),$$

where V_e is the elution volume of the sample. The hydrodynamic radius r is given by

$$r = a_0 + b_0 erf^{-1}(1 - K_{av}),$$

where a_0 and b_0 are constants of the column and erf^{-1} the inverse standard error function, found in probability tables.

Oxonol VI fluorescence measurement

Fluorescence intensity of the E_m probe oxonol VI (50 nM) was measured at excitation/emission wavelengths of 614/646 nm with an Aminco-Bowman Serie 2 spectrofluorometer, fitted with a stirred disposable cuvette (2 ml of assay medium) thermostated at 30°C. Diffusion E_m was created by adding a concentrated aliquot of K_2SO_4 (final concentration of 100 mM) to the assay medium containing reconstituted vesicles (50 μg ml^{-1} phospholipids), 20 nM valinomycin, 0.1 M HEPES-Li (pH 7.4), 50 mM Li_2SO_4, and the same K_2SO_4 concentration as that used for reconstitution (0–50 mM). E_m was determined as described in Results from four fluorescence intensities, F_{buf}, F_w, Ft_{Em}, and Ft_0 (see Fig. 1), corrected for dilution due to addition of successive aliquots. Intrinsic fluorescence of the assay buffer (F_{buf}) was substracted from F_w, Ft_{Em}, and Ft_0 before introducing these latter in relations detailed in Results or Appendix.

Protein determination

Proteins were determined according to Schaffner and Weissmann (1973), with bovine serum albumin as standard.

Statistics

All values reported in this study are the means ± SE of at least six values from two or more different membrane preparations.

RESULTS AND ANALYSIS

Response of oxonol VI to K^+-valinomycin diffusion potentials

Upon binding to lipidic vesicles, fluorescence of the lipophilic dye oxonol VI is red shifted and its quantum yield strongly increases (Bashford et al., 1979; Apell and Bersch, 1987). As the most permeant cyanine dye, oxonol VI freely equilibrates across biological membranes (Bashford et al., 1979; Clarke and Apell, 1989). After vesicle addition, a first fluorescence augmentation at 646 nm upon excitation at 614 nm (F_0) was observed in response to the oxonol VI binding on the two bilayer leaflets of vesicles at zero E_m (Fig. 1). F_0 was routinely measured after addition of the Li^+ ionophore eth (ETH 149) to Li^+-loaded vesicles, ensuring a zero E_m. In the presence of the K^+ ionophore valinomycin, imposition of an inward K^+ diffusion gradient positively polarized the vesicles and caused another fluorescence increase (ΔF) due to its additional binding onto the internal bilayer leaflet (Fig. 1) in response to the accumulation of the free form of the oxonol VI anion in the vesicle lumen. The latter was expected to accumulate according to the Nernst equilibrium (Bashford et al., 1979; Clarke and Apell, 1989):

$$Ox_1 = Ox_o \exp[(F/RT)E_m], \quad (1)$$

where R and F are the classical thermodynamic constants, T is the absolute temperature, and Ox_1 and Ox_o are the free dye concentrations in the lumen and in the outside, respectively. Classically, E_m is estimated from the fluorescence ratio ($Rt = \Delta F/F_0$) (Apell and Bersch, 1987; Venema et al., 1993; Ros et al., 1995).

PM proteins from plant root cells were reconstituted in mixed soybean phospholipids or in mixed soybean phospholipid:egg PC (8:2, w/w). The 3.5-fold increase of the half-time of Rt dissipation (Fig. 2) indicated that the membrane tightness was significantly improved by complementing mixed soybean phospholipids with egg PC.

The initial fluorescence ratio (Rt_i) was measured at increasing K^+-valinomycin gradients and plotted versus K^+-Nernst potentials (E_{Nernst}, Fig. 3). Unexpectedly, Rt_i reached a plateau (Rt_{max}) at E_{Nernst} larger than 130–150 mV. This could arise from 1) free dye depletion as the assay medium contained only 50 nM oxonol VI or 2) saturation of the internal membrane leaflet and/or quenching of bound dye at high E_m (oxonol V is quenched upon E_m generation; Kaestner and Sze, 1987).

Binding parameters were determined by titrating oxonol VI (50 nM) with liposomes and reconstituted PM vesicles (Fig. 4). Scatchard plots were linear, indicating that oxonol VI binding obeyed a mass action law (Fig. 4, inset). Maximal (extrapolated) fluorescence for totally bound dye (Fm_{lip}, Table 1), compared with $F_0 + \Delta F$ previously observed at Rt_{max} (Fig. 1 or 2), indicated that 60% of oxonol molecules remained free at the plateau; therefore, the Rt_{max} value could not be related to dye depletion. Second, liposomes and reconstituted PM vesicles were titrated with oxonol VI

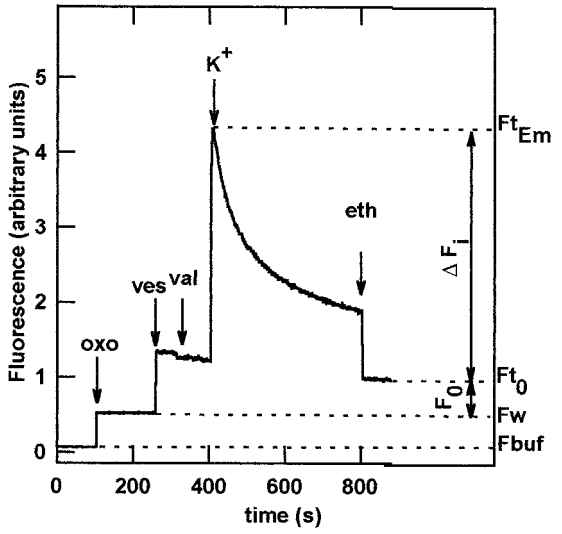

FIGURE 1 Typical fluorescence response of oxonol VI to the imposition of an infinite inward K^+-valinomycin diffusion gradient across control liposomes. Liposomes were prepared in a Li^+-containing reconstitution buffer without K^+, as described in Materials and Methods. At the indicated times, oxonol VI (oxo = 50 nM), liposomes (ves = 50 μg phospholipid ml^{-1}), valinomycin (val = 20 nM), K_2SO_4 (K^+ = 100 mM), and the Li^+ ionophore eth (2 μM) were successively added. E_m was determined from four fluorescence intensities: 1) the (intrinsic) fluorescence of the assay medium (F_{buf}), 2) the total fluorescence after oxonol addition (F_w), 3) the one after imposition of a positive inside E_m using K^+-valinomycin diffusion gradients (Ft_{Em}), 4) the one at zero E_m, measured after short-circuiting E_m with Li^+-ionophore eth (Ft_0). Addition of vesicles and imposition of E_m led to two increases of the fluorescence, respectively, noted F_0 ($F_0 = Ft_0 - F_w$) and ΔF ($\Delta F = Ft_{Em} - Ft_0$), due to the oxonol VI binding to the membrane. The maximal, initial ΔF is noted ΔF_i. Fluorescence intensities were corrected for successive dilutions.

(Fig. 5). Linear Scatchard plots indicated that the quantum yield of the dye remained constant throughout binding isotherms (Fig. 5, inset). Maximal (extrapolated) fluorescence per saturated membrane leaflet ($Fm_{ox}/2$, Table 1) was 11- to 18-fold higher than the value of $F_0 + \Delta F$ observed at Rt_{max}. Thus, the latter could not be related to the saturation of the internal leaflet or to the quenching of bound dye.

Alternatively, we hypothesized that diffusion E_m could not exceed 140 mV. Dielectrical breakdown seemed unlikely because it is known to occur within 250–300 mV in plant cells (Teissie and Tsong, 1981; Mueller et al., 1983) and because the half-time of Rt dissipation remained constant at E_{Nernst} of 73 mV, 116 mV, 192 mV, and even infinite (when the vesicle lumen was initially deprived of K^+; inset of Fig. 3). Diffusion E_m across small vesicles could be otherwise limited by the high capacitance (C_m) of biological membranes (Apell and Bersch, 1987). Indeed, charging the equivalent membrane capacitor so that E_m increases from 0 to E_{m_i} (corresponding to Rt_i), requires that a significant number of K^+ ions enter into the vesicle lumen. Because the small vesicle size, this initial entry of K^+ significantly increases the internal K^+ concentration from K^+_{li} (initially imposed) to K^+_{lf} (finally reached at equilibrium $E_m = E_{m_i}$). E_{m_i} should be reached for $K^+_{lf} = K^+_{li} +$

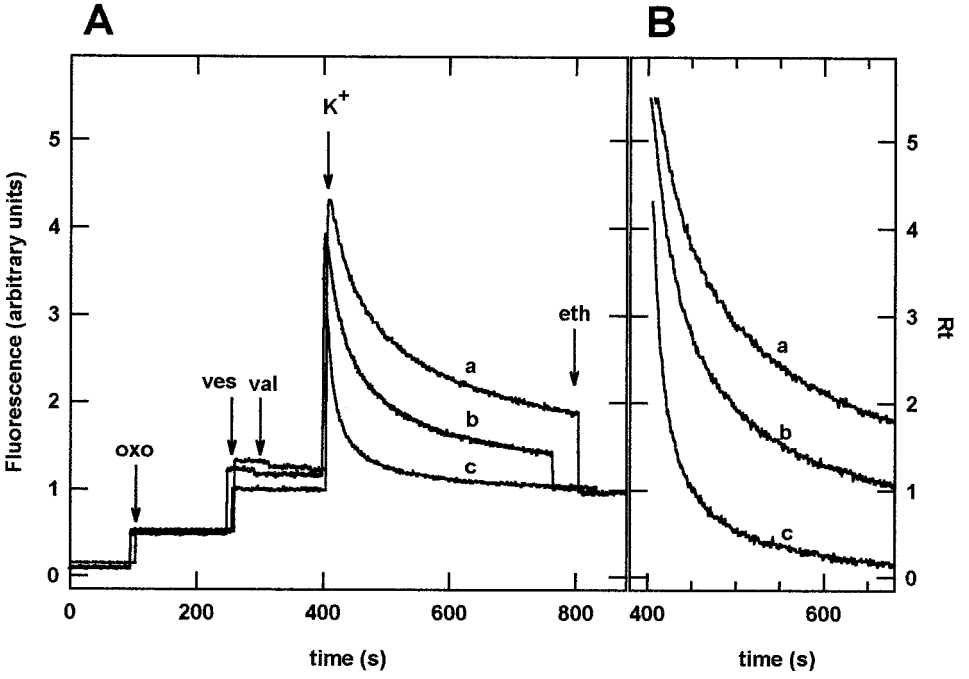

FIGURE 2 Effect of egg PC complementation of mixed soybean phospholipids on the tightness of reconstituted PM vesicles. Experimental conditions for E_m imposition were similar, and labels have the same meaning as the ones in the legend of Fig. 1. (*A*) Responses of liposomes (*trace a*) and reconstituted PM vesicles (*trace b*), both prepared from mixed soybean phospholipids complemented with egg PC (8:2, w/w), as described in Materials and Methods. *Trace c* corresponds to PM vesicles reconstituted from soybean phospholipids without egg PC. The fluorescence ratio Rt ($Rt = \Delta F/F_0$; see Fig. 1) obtained from data in *A* is plotted in *B*. Half-time of the decay kinetics of Rt increased from 14 to 48 s when mixed soybean phospholipids were complemented with egg PC for protein reconstitution.

K^+_{eq}, the latter being expected from the classical relation $Q = AC_mE_m$, where A and Q are the capacitor area and charge, respectively:

$$K^+_{eq} = Q/(FV) = 3C_mE_{mi}/(R_vF), \quad (2)$$

where R_v and V are the vesicles radius and volume, respectively.

$$E_{mi} = (RT/F)\ln[K^+_o/(K^+_{li} + K^+_{eq})] \quad (3)$$

$$3C_mE_{mi}/(R_vF) + K^+_{li} - K^+_o \exp[-(F/RT)E_{mi}] = 0 \quad (4)$$

Equation 4 can be solved numerically to calculate E_{mi} from initially imposed K^+_o/K^+_{li} gradients (Apell and Bersch, 1987). Noteworthy, it gives maximal $E_{mi} = 125$ mV for the highest used K^+_o in the present study (200 mM, Fig. 3) and for $K^+_{li} = 0$, using $R_v = 28$ nm (Table 2) and $C_m = 1$ μF cm^{-2} (Schatchtman et al., 1991; Sukhorukov et al., 1994). Thus, the capacitor model accounted for the plateau Rt_{max} observed at E_{Nernst} larger than 140 mV (Fig. 3). From Eq. 2, K^+_{eq} corresponding to this maximal E_m was 1.3 mM. As confirmed by comparison of E_{Nernst} and experimental E_m (E_{probe3}, Fig. 6 *A*) determined as indicated below, E_{Nernst} calculated from initially imposed K^+_o/K^+_{li} (as opposed to K^+_o/K^+_{lf}) appeared misleading for K^+_{li} lower than or close to K^+_{eq}, due to capacitor properties of vesicles (Fig. 6 *B*).

Direct determination of E_m with oxonol VI

As calibration using E_{Nernst} calculated from K^+_o/K^+_{li} could be misleading, E_{mi} was determined directly from oxonol VI Rt_i. As a permeant lipophilic anion, the free form of oxonol VI is expected to thermodynamically equilibrate across the membrane vesicle according to Eq. 1 (Bashford et al., 1979; Apell and Bersch, 1987). Although the response of Rt_i to E_{mi} arises from that of the bound and not of the free form of the dye, E_{mi} was determined using Eq. 1 assuming that 1) oxonol VI binding to the two membrane leaflets was linear with free oxonol VI concentration, which was likely because its total concentration (50 nM) was 100-fold lower than the dissociation constant of membrane sites ($K_d = 6$ μM; Fig. 5 and Table 1) and 2) free external dye concentration (Ox_o) remained nearly constant and equal to the total concentration; it was estimated above that 60% of the dye remained free at maximal E_{mi}.

From these hypotheses, the accumulation ratio of the bound dye on the two bilayer leaflets (Ox_{bl}/Ox_{bo}) was expected to be linear with the one of the free dye in the two compartments (Ox_l/Ox_o), and therefore the former ratio could be used in place of the latter to calculate E_{mi} using Eq. 1. From the definition of ΔF and F_0 indicated in Fig. 1, Ox_{bl} and Ox_{bo} were proportional to ($\Delta F + F_0/2$) and $F_0/2$, respectively, and E_{mi} given by

$$E_{mi} = (RT/F)\ln(2Rt_i + 1) \quad (5)$$

This first direct estimate of E_{mi} is denoted E_{probe1} in the following. In experiments of Fig. 6, E_{mi} was adjusted by varying K^+_{li} at constant $K^+_o = 200$ mM. As smaller E_{mi} corresponded to $K^+_{li} \gg K^+_{eq}$, as required to escape to capacitor effects evoked above, E_{probe1} was expected to be initially linear (with a slope of 1) with E_{Nernst} calculated from K^+_o/K^+_{li}. In addition, maximal E_{probe1} was expected to be ~120–130 mV according to Eq. 4. Indeed, E_{probe1} was initially linear with E_{Nernst} (Fig. 6) as opposed to the classical plot Rt_i versus E_{Nernst}, which was sigmoidal (Fig. 3). However, both slope and maximal E_{probe1} were approximately twofold smaller than that expected.

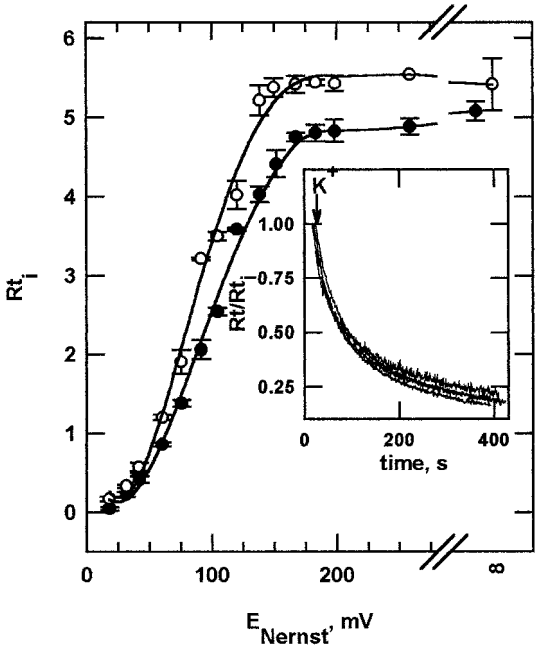

FIGURE 3 Effect of increasing K^+-valinomycin diffusion gradient on the initial fluorescence ratio of oxonol VI. Vesicles were reconstituted in the presence of 0–50 mM K_2SO_4 and equilibrated in the assay medium containing the same K_2SO_4 concentration, in the presence of valinomycin. Then, positive E_m was generated as described in Fig. 1 by adding a concentrated aliquot of K_2SO_4 to give a final external concentration of 100 mM. The mean value of the initial fluorescence ratio ($Rt_i = \Delta F_i/F_0$), and the associated standard error determined from four to six experiments with reconstituted PM vesicles (●) or liposomes (○), is plotted versus the Nernst potential expected from the K^+-diffusion gradient initially imposed ($E_{Nernst} = (RT/F)\ln(K_o^+/K_i^+)$). (*Inset*) Decay kinetics of Rt/Rt_i for reconstituted PM vesicles at following E_{Nernst}: 73 mV, 116 mV, 192 mV, and infinite (no K^+ initially inside).

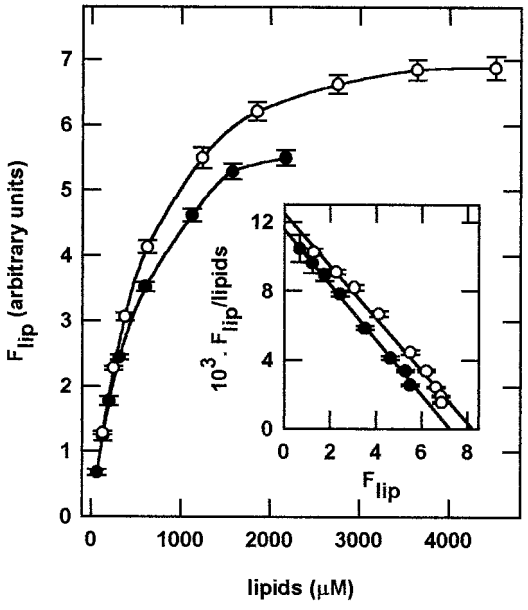

FIGURE 4 Fluorescence titration of oxonol VI with reconstituted PM vesicles and liposomes at zero E_m. Medium contained 50 nM oxonol VI in 0.1 M HEPES-Li (pH 7.4), 50 mM Li_2SO_4, 0.5 mM K_2SO_4, and the indicated phospholipid concentrations. PM vesicles (●) or liposomes (○) were reconstituted in the same buffer, as described in Materials and Methods. F_{lip} is the oxonol fluorescence increase after each vesicle addition, due to the binding of the probe onto these latter. F_{lip} was corrected for the fluorescence of free oxonol and the intrinsic fluorescence of the vesicles, measured in separate experiments. The maximal F_{lip} values (Fm_{lip}) extrapolated from the linear Scatchard plot (*inset*) are given in Table 1. Fm_{lip} allows the calculation of the ratio of the relative fluorescence yield of oxonol (Φ_r) when bound on the vesicles relative to free in solution (see text and Table 1).

The major part of this discrepancy arose from the significant depletion of the free dye upon increasing E_{mi}, in contradiction with the second hypothesis above. This effect was accounted for, as detailed in the Appendix, from the fluorescence intensities F_w, Ft_0, and Ft_{Em}, measured in each record (Fig. 1), and from the relative fluorescence yield Φ_r of bound/free dye, determined from titrations above (see legend of Table 1). Rt_i corrected for depletion, and denoted Rt_i'', was given by

$$Rt_i'' = F_w((Ft_{Em} - Ft_0)(\Phi_r - 1))/((\Phi_r F_w - Ft_{Em})(Ft_0 - F_w)) \quad (6)$$

Introducing Rt_i'' in place of Rt_i in Eq. 5 gave E_{probe2}, initially linear with E_{Nernst} with a slope close to 1 (0.85) and maximal E_{probe2} close to 115 mV (Fig. 6). In addition, data were corrected for the slight deviation from linearity of the bound versus free dye relation (see first hypothesis above), expected to occur at the internal and not external leaflet. Indeed, in the latter case, Ox_{bo} remained likely linear with Ox_o because the latter (50 nM) was at least 100-fold lower than membrane site K_d (6 μM; Fig. 5 and Table 1) whatever E_{mi}, as already noted. By contrast, Eq. 1 predicted that Ox_l could increase up to 6 μM at maximal expected E_{mi} (130 mV), and thus Ox_{bl} versus Ox_l likely deviated from linearity at the highest E_{mi} values.

The binding isotherm of oxonol VI can be accounted for (see the Appendix) by the values of K_d and number of sites per lipid (N, Table 1) and the lipid concentration (*Lip*). This allowed us to determine the nonlinear relationship between the ratio Ox_{bl}/Ox_{bo}, experimentally given by $2Rt_i'' + 1$, and the ratio Ox_l/Ox_o used to calculate equilibrium E_{mi} in Eq. 1.

TABLE 1 Oxonol VI binding and fluorescence parameters

Vesicle type	Fm_{lip} (a.u.)	Φ_r	Fm_{ox} (a.u.)	K_d (μM)	N (mol mol^{-1})
Liposomes	8.2	17.2	85.6	6.2	8.3×10^{-3}
Proteoliposomes	7.3	15.1	124.9	7.4	13.8×10^{-3}

The parameter Fm_{lip} was the maximal fluorescence intensity of bound oxonol VI (50 nM), determined by extrapolating the linear Scatchard plot of data from titration with membrane vesicles (Fig. 4). Φ_r is the relative fluorescence yield ($\Phi_r = Fm_{lip}/F_w$, where F_w is the fluorescence intensity of 50 nM free oxonol in buffer, measured in the same conditions; see Fig. 1). Parameters Fm_{ox} and K_d were, respectively, the maximal fluorescence intensity at oxonol VI saturation of membrane vesicles (63 μM phospholipids), and the dissociation constant of membrane sites, determined by extrapolating the linear Scatchard plot of data from titration with oxonol VI (Fig. 5). The specific number of membrane sites (N, mol per mol of phospholipids) was given by $N = Fm_{ox}Oxt/(Fm_{lip}\,Lip)$, where *Lip* is the concentration of vesicle phospholipids. a.u., arbitrary units.

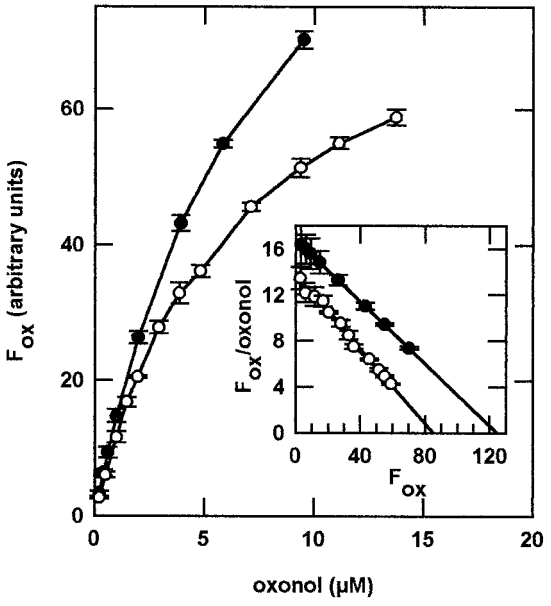

FIGURE 5 Fluorescence titration of reconstituted PM vesicles and liposomes with oxonol VI at zero E_m. The assay medium contained 0.1 M HEPES-Li (pH 7.4), 50 mM Li_2SO_4, 0.5 mM K_2SO_4 plus a fixed concentration of membrane vesicles (63 μM phospholipid). Reconstituted PM vesicles (●) and liposomes (○) were reconstituted in the same buffer, as described in Materials and Methods. The value of F_{ox}, due to the oxonol VI binding on membrane vesicles, is the total fluorescence observed after dye addition minus the corresponding one measured for free oxonol in separate experiments. When the absorbance of the dye was higher than 0.05, the fluorescence intensity was corrected for inner filter quenching according to the method of Beyer et al. (1972). The dissociation constant and the maximal value of F_{ox} (Fm_{ox}), extrapolated from the linear regression of the Scatchard plot (*inset*), were, respectively, 6.2 μM and 85.6 for liposomes, and 7.4 μM and 124.9 for reconstituted PM vesicles. The number (N) of binding sites per phospholipid unit was calculated from Fm_{ox} (see Table 1).

As detailed in the Appendix, E_{mi} given by the probe after correction for depletion and saturation effects, denoted E_{probe3}, was given by

$$E_{probe3} = (RT/F)\ln[\{2Rt_i'' + 1\}/\{1 - (Oxt(2Rt_i'' + 1) \cdot (Ft_{Em} - F_w))/(N\,Lip\,F_w(Rt_i'' + 1)(\Phi_r - 1))\}] \quad (7)$$

The initial slope of the linear regression of E_{probe3} versus E_{Nernst} in the range 0–130 mV reached the expected value (Fig. 6), and the E_{probe3} plateau (125 mV) agreed with maximal E_{mi} calculated with Eq. 4 accounting for diffusion E_m across capacitor vesicles.

Maximal E_{probe3} measured for liposomes of different sizes (Table 2) confirmed that maximal E_{mi} increases with the vesicle radius, as expected from Eq. 4. Furthermore, maximal E_{probe3} agreed with maximal E_{mi} calculated with this relation, confirming that 1) the capacitance of the biological membrane actually limits the magnitude of diffusion E_m across microscopic vesicles (Apell and Bersch, 1987) and 2) the actual E_m can be reliably determined from oxonol VI fluorescence with Eq. 7, independently of the E_{Nernst} calibration, which is misleading at high E_m. In the following, E_m stands for E_{probe3} given by oxonol VI as described above.

Determination of net passive nitrate and proton fluxes and permeability coefficients

Addition of NO_3^- (15 mM) to the external medium of reconstituted PM vesicles strongly increased the dissipation rate of the oxonol VI response to K^+-valinomycin diffusion gradient (K_o = 200 mM as SO_4^{2-} or SO_4^{2-}:NO_3^- salt; K_{li} = 1 mM as SO_4^{2-} salt), whereas it had nearly no effect on the initial response (Fig. 7 *A*). We showed that NO_3^- only slightly increased the dissipation rate of the oxonol VI response to a similar K^+-valinomycin diffusion gradient across control liposomes (Grouzis et al., 1997). Thus, insertion of PM proteins into the lipid bilayer, although 15-fold (w/w) diluted at the surface of membrane vesicles after reconstitution, appeared to induce a large NO_3^- leak. In addition, the desired information, i.e., the net passive NO_3^- flux (J_N) mediated by PM protein(s), appeared contained in the NO_3^--dependent component of the dissipation kinetics of the diffusion E_m rather than in a variation of the initial value of the latter.

Therefore, J_N was determined as indicated in Fig. 7 from two main hypothesis: 1) K^+ remains at thermodynamic equilibrium across the membrane vesicle with the E_m value given independently by the oxonol dye, and 2) the kinetics of E_m dissipation underlie a net K^+ influx (J_K), which depends on the magnitudes of H^+ and NO_3^- leaks electrically compensating the entry of K^+. The validity of hypotheses 1 and 2 is addressed in the Discussion. The first step of J_N determination consisted in calculating E_m (i.e., E_{probe3}; Fig. 7 *B*), as described in the preceding section, from fluorescence intensity (FI) records in the presence or in the absence of NO_3^- (Fig. 7 *A*). The second step consisted in calculating the K^+ concentration in the lumen (K_l; Fig. 7 *C*) during K^+ filling kinetics according to

$$K_l^+ = K_o^+ \exp[-(F/RT)E_m] \quad (8)$$

A nonlinear regression fit of $K_i^+ = f(t)$ was used to determine the polynomial equation:

$$\left(K_l^+ = \sum_{j=0}^{n} k_j t^j\right),$$

accounting for the K^+ filling kinetics. Finally, J_K (Fig. 7 *D*) was obtained from the derivative:

$$dK^+ = \sum_{j=1}^{n} j k_j t^{j-1}$$

and the equation:

$$J_K = d(K_l^+ V)/(A dt) = (R_v/3)dK_l^+/dt \quad (9)$$

According to the second hypothesis above, J_K was considered as electrically compensated either by a net H^+

TABLE 2 Vesicle size and maximal diffusion E_m

	Pyranine		Gel chromatography		Oxonol VI
Liposome type	r* (nm)	E_m calculated (mV)	r (nm)	E_m calculated (mV)	E_m measured (mV)
Reconstituted	28 ± 2	129 ± 2	32 ± 10	131 ± 10	125 ± 6
Sonicated	44 ± 5	139 ± 4	55 ± 10	143 ± 6	148 ± 3
Freeze-thawed	ND	ND	185 ± 20	171 ± 4	170 ± 3

Various types of liposomes were prepared, and corresponding radius (r) was estimated using gel exclusion chromatography or entrapped pyranine fluorescence measurements, as described in Materials and Methods. Introducing r in the vesicle capacitor model (Eq. 4) allowed us to calculate the maximal diffusion potential (E_m calculated) as a function of r, for comparison with the one measured with oxonol VI (E_m measured = E_{probe3}; Eq. 7) after imposition of an infinite inward K^+-valinomycin diffusion gradient.

*Internal radius given by the pyranine dye plus 5 nm (to account for the membrane thickness).

efflux (J_H) in the absence of NO_3^- or by both a net H^+ efflux and a net NO_3^- influx (J_N) in its presence. Therefore, denoting $(J_K)_N$ and $(J_K)_{0N}$ the values of J_K in the presence or in the absence of NO_3^-, J_N and J_H were given as

$$J_N = (J_K)_N - (J_K)_{0N} \text{ and } J_H = (J_K)_{0N} \quad (10)$$

Permeability coefficients were calculated from J_N or J_H and E_m using the Goldman-Hodgkin-Katz (G-H-K) relation (Stein, 1986). For reasons detailed in Discussion, only initial values of E_m and fluxes were considered in the following (noted E_{mi}, J_{Hi}, J_{Ni}). As NO_3^- was added initially to the outside ($NO_{3\,o}^-$) of vesicles deprived in this anion, the G-H-K relation could be simplified to calculate the permeability coefficient (P_N):

$$P_N = -J_{Ni}[RT/(zFE_m)][1 - \exp\{z(F/RT)E_m\}]/NO_{3\,o}^- \quad (11)$$

As both internal and external pH were the same, the G-H-K relation could be also simplified to calculate the permeability coefficient for H^+ (P_H):

$$P_H = -J_{Hi}[RT/(zFE_m)]/10^{-pH} \quad (12)$$

In the experiment in Fig. 7, with reconstituted PM vesicles, J_{Ni} was 4.7×10^{-9} mol m^{-2} s^{-1} corresponding to P_N of 8.6×10^{-11} m s^{-1}, according to Eq. 11. By contrast, a 10^4 higher value was obtained for P_H (10^{-6} m s^{-1}) from J_{Hi} (1.2×10^{-9} mol m^{-2} s^{-1}), according to Eq. 12. As a similar high P_H was obtained with control liposomes (0.8–0.9×10^{-6} m s^{-1}), it is likely that J_{Hi} in reconstituted PM vesicles occurred by diffusion across the lipid bilayer, rather than by a protein-facilitated transport. P_N of reconstituted PM vesicles and liposomes, at two pH values and at low (50–60 mV) or high (90–100 mV) E_m, are indicated in Table 3. The P_N of liposomes remained close to 1.7×10^{-11} m s^{-1} at the two pH and E_m values, indicating the adequacy of the G-H-K model to account for the NO_3^- diffusion across a lipid bilayer. The P_N of reconstituted PM vesicles was only 20–30% higher than that of liposomes at low E_m, whereas it was fourfold higher at pH 6.5 and high E_m. The protein-facilitated component of J_{Ni}, estimated as J_{Ni} of reconstituted PM vesicles minus J_{Ni} of control liposomes, was linear with the protein to lipid ratio (w/w) within the usable range (0.04–0.1; Table 3). Accounting for the surface dilution of proteins in the lipid bilayer after reconstitution, and for the protein to lipid ratio (w/w) close to 1 reported for native corn root PM (Gronewald et al., 1982), the P_N of the latter should be $\sim 1.2 \times 10^{-9}$ m s^{-1} at pH 6.5 and E_m within 90–100 mV, 70-fold higher than the P_N of control liposomes.

DISCUSSION

Structural effects on diffusion E_m across vesicles

The present study confirms that capacitor properties of biological membranes restricts the maximal diffusion E_m across microscopic vesicles, due to their high surface to volume ratio, as shown by Apell and Bersch (1987). E_m smaller than E_{Nernst} expected from the initially imposed diffusion gradient K_o^+/K_{li}^+ are observed when K_{eq}^+, the equivalent concentration of K^+ ions transferred inside to polarize the vesicle capacitor, is not negligible as compared with K_{li}^+ (Fig. 6 *B*). Maximal K_o^+ was 200 mM in the present study. Using this concentration, and vesicles loaded with 0.1 mM K_{li}^+ (expected E_{Nernst}, 185 mV), oxonol VI indicated that E_m reached 120 mV (Fig. 6), in accordance with equilibrium E_m for $K_I^+ = K_{li}^+ + K_{eq}^+ = 0.1$ mM + 1.3 mM, expected from the capacitor model (Eqs. 2, 3, and 4). This explains the increasing discrepancy observed above 70 mV (Fig. 6) between E_m indicated by the dye and expected E_{Nernst}. Published E_m values determined from the measured accumulation ratio of radiolabeled lipophilic ions (by applying Eq. 1) are generally smaller than expected E_{Nernst} at the larger used diffusion gradients (for example, Marshall et al., 1994; Huang et al., 1994), and this discrepancy seems explainable by the capacitor model (not shown). Agreement between maximal E_m indicated by oxonol VI for vesicles of different sizes and maximal E_m calculated from the capacitor model (Table 2) confirms the adequacy of the latter to account for such discrepancies.

The net negative electrostatic charge (σ) displayed by the membrane surface, due to fixed ionized groups, appeared as another structural property that affects E_m, i.e., the electrical potential difference between the two bulk solutions. E_m is known to include an electrostatic component, besides the diffusive one, corresponding to the difference of the inner and outer electrostatic (surface) potentials (Ohki, 1981).

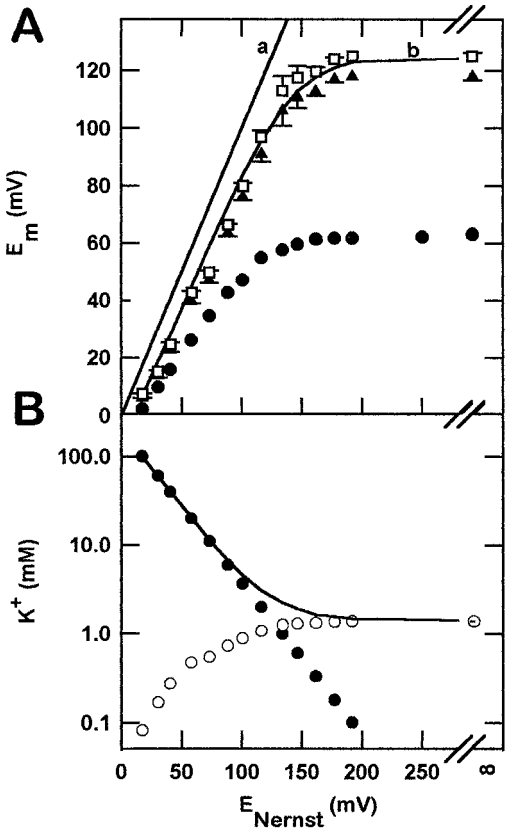

FIGURE 6 K^+-valinomycin diffusion gradients across reconstituted PM vesicles or control liposomes: comparison of experimental potentials given by the oxonol VI probe and expected K^+ Nernst potentials. (*A*) The diffusion potential in response to increasing K^+-valinomycin gradients was experimentally determined (E_m) from the oxonol VI fluorescence and plotted versus the Nernst potential expected from the initially imposed K^+-valinomycin gradient ($E_{Nernst} = (RT/F)\ln(K_o^+/K_{li}^+)$). Three experimental E_m estimates were calculated (Eq. 5) from the fluorescence ratio $Rt_i = \Delta F_i/F_0$, measured as described in Fig. 1 and shown in Fig. 3: E_{probe1} (●) calculated from Rt_i without any correction; E_{probe2} (▲) from Rt_i corrected for dye depletion (Eq. 6); E_{probe3} (□) from Rt_i corrected for both dye depletion and dye saturation of the internal vesicle leaflet (Eq. 7). Reference E_{Nernst} values are also plotted (*curve a*) to facilitate comparison. *Curve b* corresponds to the theoretical potential expected from capacitive effects on diffusion potential across membrane vesicles (Eq. 4, with C_m = 1 μF cm^{-2}, r = 28 nm; see Materials and Methods and Table 2); the K^+ concentrations in the lumen (K_l^+) introduced in this calculation were those at equilibrium with the negative-inside Donnan potential expected before the imposition of the K^+ gradient (Eq. 8). (*B*) Comparison of the K^+ concentration initially present in the lumen of the vesicles (K_{li}^+, ●) and the equivalent K^+ concentration to be transferred in the lumen to charge the membrane capacitor according to Eq. 2 (K_{eq}^+, ○); the solid line indicates the total internal concentration of K^+ ($K_l^+ = K_{li}^+ + K_{eq}^+$) theoretically expected at initial equilibrium E_m; the increasing discrepancy between E_{probe3} and E_{Nernst} is observed (see *A*) when K_{eq}^+ becomes significant compared to K_{li}^+.

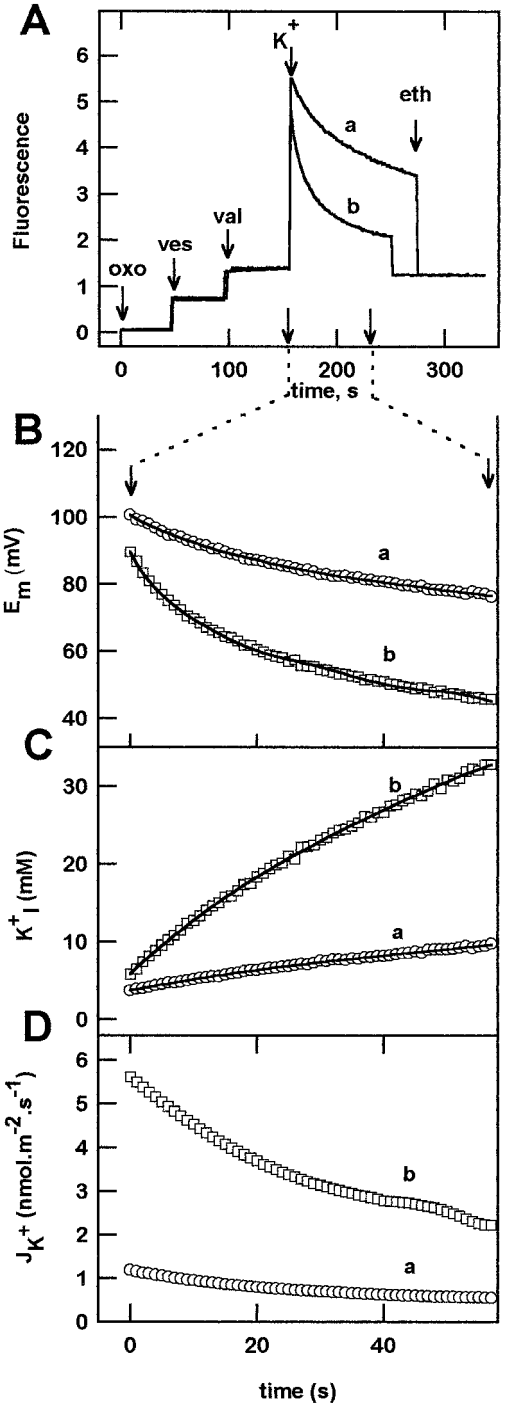

FIGURE 7 Determination of net ion fluxes from depolarization kinetics of K^+-valinomycin diffusion potentials. (*A*) Fluorescence records at pH 6.5 after successive additions of oxonol VI, reconstituted PM vesicles, valinomycin, and K_2SO_4 (*trace a*), or K_2SO_4 plus KNO_3 (*trace b*), to make the final concentration of K^+ and NO_3^- equal to 200 mM and 15 mM, respectively. The Li^+-ionophore eth was added at the end of the assay to clamp E_m to zero, both external and internal media containing Li^+. (*B*) E_m (E_{probe3}, Eq. 7) was calculated from the four fluorescence intensities indicated in Fig. 1. (*C*) Internal K^+ concentration (K_l^+) at equilibrium with E_m was calculated (Eq. 8) and fitted using a polynomial regression algorithm (solid line). (*D*) Net K^+ fluxes (J_K) in the presence and in the absence of NO_3^- were calculated from the derivatives of the polynomial fits (Eq. 9), and the net NO_3^- flux (J_N) was determined as the NO_3^--dependent augmentation of J_K (see text).

High electrostatic potentials have been demonstrated at the soybean liposome interface, reaching −100 mV at 1 mM ionic strength (Schlieper et al., 1981). In the present study, a high ionic strength was used in both external/internal medium (50 mM Li_2SO_4, 100 mM HEPES-Li at pH 7.4) to attenuate surface potentials via the so-called screening effect. The Gouy-Chapman theory is adequate to describe

TABLE 3 Permeability coefficient to NO_3^- of liposomes and reconstituted PM vesicles

Vesicles	pH	E_m (mV)	J_{Ni} (nmol m^{-2} s^{-1})	P_N (m s^{-1} 10^{11})
Liposomes	6.5	95 ± 4	0.97 ± 0.09	1.72 ± 0.01
Liposomes	6.5	53 ± 2	0.62 ± 0.04	1.76 ± 0.09
Liposomes	7.4	94 ± 5	0.97 ± 0.06	1.73 ± 0.04
Liposomes	7.4	52 ± 2	0.59 ± 0.04	1.71 ± 0.13
Proteoliposomes	6.5	99 ± 3	4.60 ± 0.44	7.86 ± 0.69
Proteoliposomes	6.5	56 ± 1	0.84 ± 0.01	2.31 ± 0.02
Proteoliposomes	7.4	99 ± 4	1.76 ± 0.27	3.04 ± 0.55
Proteoliposomes	7.4	55 ± 1	0.83 ± 0.07	2.31 ± 0.19
Proteoliposomes	6.5	90 ± 6	7.12 ± 0.91	13.3 ± 2.31
Proteoliposomes	6.5	94 ± 4	3.50 ± 0.42	6.35 ± 0.61

Liposomes and reconstituted PM vesicles (proteoliposomes) were prepared as described in Materials and Methods. Proteoliposomes were formed at a lipid to protein ratio (w/w) of 15, except in the last two listed, corresponding to ratios of 10 and 25, respectively. Net initial fluxes of nitrate (J_{Ni}) in vesicles were determined at pH 6.5, or pH 7.4, from the NO_3^--dependent (15 mM NO_3^-) augmentation of the depolarization rate of the K^+-valinomycin diffusion potential, as described in the text and accompanying figures and legends. Initial E_m was adjusted to the indicated value by varying the K^+-diffusion gradient. Permeability coefficient to NO_3^- (P_N) was calculated from the Goldman-Hodgkin-Katz relation (Eq. 11).

electrostatic potential and ion screening effect at the biological membrane interface; noteworthy, potentials ~−20 mV are observed at such ionic strength (Gibrat and Grignon, 1983). Nevertheless, E_m is not expected to include an electrostatic component (or a diffusive one) when the same electrolyte solution, in principle, bathes both leaflets of symmetrical membranes as used in the present study, as both inner and outer surface potentials are in theory identical. To explain the small, negative-inside, E_m indicated by the oxonol dye in such a situation (see the *y* axis intercept of the experimental curve in Fig. 6), we hypothesized that the electrostatic field of the inner surface may overlap in the core of the vesicles, owing to their small size. However, the Gouy-Chapman theory does not allow us to describe this situation, and we used the Donnan theory for the sake of simplicity (Lakshminarayanaiah, 1984). The latter theory gives a simple explanation frame of the phenomenon, considering fixed surface charges as nonpermeant charges randomly distributed in the inner and outer compartments. In contrast to the outer compartment, where unpermeant charges may be considered as infinitely diluted, the small inner lumen should enclose a high concentration of the latter and therefore a significant and stable excess of diffusive counterions (cations) responsible for a negative-inside equilibrium Donnan potential given by

$$E_{Donnan} = (RT/F)\text{argsinh}(272\sigma/C^{1/2}), \qquad (13)$$

where C is the concentration of monovalent salt and σ the net electrostatic charge. Indeed, the experimental E_{probe3} curve in Fig. 6 extrapolated to a small negative $E_m = -10$ mV in the absence of imposed K^+ diffusion gradient, in agreement with the E_{Donnan} value given by Eq. 8 (−11 mV, with $C = 0.2$ M K^+ plus 0.144 M Li^+ inside and $\sigma = 10^{-3}$ elementary charge $Å^{-2}$) (Schlieper et al., 1981). In the experiment described in Fig. 6, vesicles were first equilibrated in the presence of valinomycin and $K_o^+ = K_{li}^+$ before adding a concentrated K_2SO_4 aliquot to generate E_m at final $K_o^+ = 200$ mM. To account for the small electrostatic component, E_m was calculated as previously indicated according to the vesicle capacitor model, except that the Donnan equilibrium $K_{li'}^+$ ($K_{li'}^{+'} = K_{li}^+ \cdot \exp\{-(F/RT)\, E_{Donnan}\}$) was introduced in Eq. 4 in place of K_{li}^+ initially imposed. The E_m calculated in this way correctly described E_{probe3} (Fig. 6, *line b*).

In conclusion, ionophore-mediated diffusion E_m across microscopic vesicles is structurally limited by the capacitor properties of biological membranes. As shown in Fig. 6, the E_m range usable from such diffusion gradients lies within 0–130 mV. This overlaps with the physiological range of the E_m of animal cells (Hille, 1992) but only partially with that of plant cells (Sanders and Slayman, 1989). Therefore, the study of some solute transport systems from plant cells could be restricted; for example, recently identified inward rectifying K^+ channels (KAT1 and AKT1) are activated for (absolute) E_m larger than 100 mV (Schachtman et al., 1992; Very et al., 1995). This could be overcome in several ways: 1) use of vesicles of higher radius (Philippot et al., 1983) to diminish the surface/volume ratio (the maximal E_m should increase up to 190 mV using membrane vesicles of 1-μm diameter); 2) clamping the internal concentration of the diffusive ion (we have shown elsewhere that buffering the vesicle lumen allows us to generate H^+ diffusion E_m up to 250 mV (Ros et al., 1995)); and 3) activation of highly electrogenic pumps (Ros et al., 1995).

Probing E_m without E_{Nernst} calibration of oxonol VI

Oxonol VI can be used for quantitative and continuous monitoring of E_m without E_{Nernst} calibration, provided that experimental conditions are carefully chosen. A low oxonol concentration is required for two reasons. First, the large permeability coefficient of the lipid bilayer for the anion oxonol VI (Clarke and Apell, 1989), useful to monitor fast variations of E_m, is responsible for a partial E_m short-circuiting when the dye is used in the micromolar range. A concentration lower than 100 nM was required in our conditions (Venema et al., 1993). Second, oxonol VI fluores-

cence responds to E_m via an additional binding onto the internal membrane leaflet, at equilibrium with the free dye accumulated inside according to Nernst equilibrium (Eq. 1). Therefore, E_m can be monitored as long as internal binding sites remain unsaturated. In the present study, maximal diffusion E_m was ~120 mV, corresponding to a 100-fold accumulation (Eq. 1) of the free dye (5 μM in the lumen for 50 nM in the outside). Approximately 60% of internal sites remained unsaturated at 120 mV from comparison of maximal FI of bound oxonol (Fig. 4; Table 1) and maximal FI augmentation at 120 mV (see Results), which agreed with the K_d of membrane sites (6 μM; Fig. 5 and Table 1), and depletion of free dye (see Appendix).

E_m can be directly determined from observed FI values without E_{Nernst} calibration of the dye, by using Eq. 1 to account for thermodynamic equilibrium of freely permeant lipophilic ions across the membrane vesicle (Rottenberg, 1989). Of course, this requires that the equilibrium ratio of the free dye (Ox_l/Ox_o) can be reliably estimated from that of the bound dye (Ox_{bl}/Ox_{bo}), given by the term $2Rt_i + 1$. Although the fluorescence yield Φ_r of oxonol VI increased 15- to 17-fold upon binding onto membrane vesicles (Fig. 4 and Table 1), this increase remained too low to make the FI of the free dye negligible (F_w; see typical record in Fig. 1). In our experimental conditions, addition of membrane vesicles (60 μM lipids) caused a twofold augmentation of FI (from F_w to Ft_0), sufficient for a reliable determination of F_0, needed to estimate bound dye onto the external leaflet ($Ox_{bo} = F_0/2$). However, free dye was partially depleted upon vesicle addition (~10%) and upon vesicle polarization (up to 40%), because a low total oxonol concentration had to be used (50 nM). The first aim of the theoretical treatment in the Appendix was to correct FI values measured in each assay (F_w, Ft_{Em}, and Ft_0; Fig. 1) for these two depletion steps. Despite its apparent complexity, Eq. 6 allows an easy correction of the fluorescence ratio Rt_i from the above FI values and Φ_r, determined independently (Fig. 4; Table 1). Thereafter, Ox_{bl}/Ox_{bo} is given by $2Rt_i'' + 1$ (see Results). Titration in Fig. 5 indicates that bound dye remained approximately linear with free dye below 1 μM; thus, Ox_{bl}/Ox_{bo} was usable in place of Ox_l/Ox_o to calculate E_m using Eq. 1 as long as accumulation ratios remained lower than 20, corresponding to E_m smaller than 80 mV.

At larger E_m, the internal leaflet became progressively saturated (40% saturation at maximal E_m of 125 mV), and Ox_l/Ox_o versus Ox_{bl}/Ox_{bo} was expected to deviate from linearity. The second aim of the treatment in the Appendix was to account for this deviation by introducing the isotherm of oxonol VI binding onto the membrane leaflet (Fig. 5). This correction (Eq. 7) was minor compared with that for depletion of free dye and required only the introduction of the number (N, Table 1), and not K_d, of binding sites. Although, as already noted, the observable E_m range for a given oxonol concentration depends on the K_d of membrane sites, this parameter is eliminated in the treatment in the Appendix, assuming that the membrane is symmetrical regarding its oxonol VI binding characteristics. Therefore, this treatment is suitable for reconstituted membrane vesicles, as used in the present study, and not native ones, which are highly asymmetric (Serrano, 1989; Verhoven et al., 1992). In addition, native PM vesicles from corn roots are leaky and had to be reconstituted to sustain large and durable diffusion E_m (Grouzis et al., 1997). The complexity of natural lipid mixtures, as mixed soybean phospholipids, offers two advantages: 1) the lipid bilayer exhibits a very low number of binding sites for amphipolar ions (0.01 mol of oxonol per mol of soybean phospholipid; Table 1), as compared, for example, with pure PC bilayer (0.25 mol of oxonol or of 8-anilino-1-naphtalenesulphonate per mol of PC; Bammel et al., 1987; Gibrat and Grignon, 1983); the electrostatic potential of such a natural lipid bilayer, E_m (see above), does not significantly vary upon binding of amphipolar ions (Gibrat and Grignon, 1983); and 2) lipid bilayers from complex natural lipid mixtures have been shown to form powerful bidimensional solvents required to reinsert the complex variety of proteins of cell membranes (Devaux, 1981).

In conclusion, Eqs. 6 and 7 correct oxonol FI values for depletion of free dye and saturation of binding sites on the internal membrane leaflet, allowing us to determine the accumulation ratio of free dye Ox_l/Ox_o from that of the bound dye Ox_{bl}/Ox_{bo}, given by the term $2Rt_i'' + 1$. Therefore equilibrium E_m can be directly calculated using the thermodynamic Eq. 1, as for other Nernstian lipophilic ions (Rottenberg, 1989). In the present study, the 0–80-mV range corresponded to the higher K^+ concentrations initially present in the lumen (K_{li}^+), making E_m unaffected by capacitor properties of membrane vesicles (see Fig. 6 *B* and above). As expected, E_m indicated by the dye (E_{probe3}) agreed in this range with E_{Nernst} calculated from the initial gradient K_o^+/K_{li}^+ (Fig. 6); the observed slope of E_{probe3} versus E_{Nernst} was 0.95, the former values being only ~10 mV lower than the latter ones. As discussed above, the electrostatic component of E_m (E_{Donnan}) was likely responsible for this small discrepancy. This agreement ascertains a posteriori the validity of the treatment used here to determine directly E_m, without dye calibration. At higher E_m, an increasing discrepancy was observed between E_{probe3} and E_{Nernst} as E_{probe3} reached a plateau, but the latter was quantitatively accounted for by capacitor properties of vesicles, as discussed above.

Distribution of K^+ across valinomycin-containing vesicles during depolarization kinetics

Dissipation kinetics of diffusion E_m across valinomycin-containing vesicles underlie K^+-filling kinetics. The K^+ concentration in the lumen (Fig. 7 *C*) was calculated from the E_m indicated by oxonol VI (Fig. 7 *B*), assuming that K^+ remains distributed at thermodynamic equilibrium (Eq. 8) during the depolarization kinetics.

Of course, K^+ was not strictly at equilibrium, as E_m dissipated. Nevertheless, we have shown in similar experi-

ments (except we used multilabeled liposomes containing valinomycin) that the K^+ concentration indicated in the lumen by a K^+ probe (PBFI, potassium-binding benzofuran isophthalate) remained virtually at Nernst equilibrium with E_m (simultaneously measured with oxonol VI) during the depolarization kinetics (Venema et al., 1993). In this study, a 0–80-mV range was used to escape to capacitor effects described above.

A strict K^+ equilibrium should correspond to constant E_m and zero J_K. Transmembrane K^+ electrochemical gradient ($\Delta\mu_K$) needed to drive the maximal observed J_K (8×10^{-9} mol m^{-2} s^{-1}, at E_m 100 mV, 15 mM NO_3^-, pH 6.5) can be calculated from the G-H-K relation (Stein, 1986). The P_K of vesicles was expected to be $\sim 5 \times 10^{-8}$ m s^{-1} considering that valinomycin could transport 10^4 K^+ ions s^{-1} (Läuger, 1980) and that each vesicle contained four valinomycin molecules. Introducing that P_K in the G-H-K relation shows that the maximal J_K indicated above was accounted for by $E_m = 99.9$ mV in place of equilibrium E_m (100 mV), corresponding to $\Delta\mu_K = 15$ J mol^{-1}. This confirms that the deviation from strict K^+ equilibrium E_m, required to explain the observed depolarization kinetics, and to drive J_K, is experimentally undetectable. As discussed in the preceding section, oxonol VI used as a direct E_m sensor allows us to determine the actual equilibrium E_m throughout the depolarization kinetics, whatever the size of structural effects evoked above (capacitance and surface charge). The value of K_i^+ during the depolarization kinetics was calculated from E_m (Eq. 8), assuming that K_o^+ remained constant as the internal volume of vesicles was negligible ($\sim$60 μM lipid vesicles, specific volume of 2 L mol^{-1} lipids).

Net H^+ and NO_3^- fluxes and permeability coefficient of PM from plant root cells

That E_m remained virtually at K^+ equilibrium during depolarization kinetics indicates that the K^+ conductance mediated by valinomycin was prominent over other ion leaks (i.e., K^+ Nernst potentials approximated E_m derived from the general G-H-K equation). Conversely, this implies that the corresponding K^+ filling kinetics were controlled by the size of ion leaks, electrically compensating the entry of K^+, and not by the K^+ conductance. Indeed, theoretical filling time expected from P_K estimated above for valinomycin-containing vesicles (5×10^{-8} m s^{-1}) should be $\sim$0.3 s at zero E_m, which is in agreement with the instant depolarization (i.e., K^+ filling) of Li^+-containing vesicles after addition of the ionophore eth to mediate a large compensatory Li^+ efflux (Fig. 7 *A*). Therefore, the analysis of depolarization kinetics in different ion conditions must allow for the dissection of protein-mediated leaks of interest.

As already noted, reconstitution of PM proteins in lipids forms highly tight vesicles (exhibiting high and sustained diffusion E_m) with symmetrical lipid leaflets, as required to determine directly E_m from oxonol VI FI values. In addition, protein reconstitution permits a surface dilution in the lipid bilayer and a relative decrease of protein-mediated ion leaks, which ensures that instant E_m value depends only on the equilibrium distribution of K^+ and in turn that J_K depends only on ion leaks.

In the absence of NO_3^-, J_{Ki} was assumed equal to J_{Hi} (Eq. 10). Indeed, as shown elsewhere using similar buffers and valinomycin-containing liposomes multilabeled with K^+, H^+, and E_m probes (Venema et al., 1993), diffusion E_m dissipates via electrically coupled 1:1 K^+/H^+ exchange fluxes in the absence of added permeant ionic species. The large permeability coefficient for H^+ of lipid bilayers calculated from J_{Ki} in liposomes ($P_H \approx 10^{-6}$ m s^{-1}, not shown) agrees with that measured from J_H monitored with pH probes (Rossignol et al., 1982).

J_{Ni} was taken as the difference of J_{Ki} in the presence and in the absence of NO_3^- (Eq. 10), leading to P_N of $\sim 1.8 \times 10^{-11}$ m s^{-1} for control liposomes. P_N values from literature are scarce, but this value is in the range of the ones obtained by Gutknecht and Walter (1981) for liposomes of different lipid compositions and ionic conditions. The data in Table 3 indicate that J_{Ni} in control liposomes increased with E_{mi} according to G-H-K equation (i.e., J_{Ni} at variable E_{mi} is accounted for by introducing a single P_N value of 1.8×10^{-11} m s^{-1}). In addition, similar P_N values were observed at pH 6.5 or 7.4.

J_{Ni} in reconstituted PM vesicles was also accounted for by a single P_N value (2.3×10^{-11} m s^{-1}) at pH 6.5 or 7.4 and low E_m (50–60 mV). But in this case, P_N strongly increased at high E_m (90–100 mV) and was higher at pH 6.5 ($\sim 8 \times 10^{-11}$ m s^{-1}) than at pH 7.4 (3×10^{-11} m s^{-1}); accounting for the surface dilution of proteins in lipid bilayer after reconstitution, P_N of root cell PM should be $\sim 1.2 \times 10^{-9}$ m s^{-1} at pH 6.5 and E_m within 90–100 mV, i.e., 70-fold higher than P_N due to NO_3^- diffusion across the lipid bilayer, and similar to P_K determined in situ for corn roots (Thibaud et al., 1986). Thus, PM from root cells displayed a strikingly large P_N, dependent on voltage, as shown by the in vivo electrophysiological study of anion channels in plant leaf guard cells (Schmidt and Schroeder, 1994; Hedrich and Marten, 1993). However, it was observed only at an acidic pH of 6.5, typical of the optimal pH of the plant PM H^+-ATPase. This is in agreement with the previous observation at pH 6.5 of a highly conductive passive NO_3^- pathway coupled to the H^+ pump (Grouzis et al., 1997). As already noted, no anion channel has been found to date in mature cortical root cells to explain large passive NO_3^- efflux transiently observed in response of various stress (for example, transplant shock; Delhon et al., 1995). The present study suggests that imposing an acidic pH in the plant cytosol might be important for such an investigation.

APPENDIX

The following symbols are used: E_m, membrane potential; E_{mi}, initial (maximal) E_m, corresponding to Rt_i; E_{Nernst}, Nernst potential (calculated for initial K^+ equilibrium); F_{buf}, fluorescence of the assay buffer (no dye,

no vesicles); F_w, fluorescence of the dye, free in buffer (no vesicles); Ft_0, fluorescence of the dye in the presence of vesicles at zero E_m; Ft_{Em}, fluorescence of the dye in the presence of vesicles at $E_m \neq 0$; Fm_{lip}, maximal fluorescence of the dye (50 nM), totally bound onto vesicles; Fm_{ox}, maximal fluorescence of the vesicles (63 μM), saturated by the dye; Rt, fluorescence ratio ($\Delta F/F_0$; see Fig. 1); Rt_{max}, maximal fluorescence ratio observed at infinite diffusion gradient; ϕ_w, fluorescence yield of free dye (equivalent to quantum yield); ϕ_{lip}, fluorescence yield of bound dye; ϕ_r, relative fluorescence yield of the dye (bound/free); *Lip*, phospholipid concentration; N, number of binding sites per unit phospholipid concentration; K_d, dissociation constant of binding sites; Ox_i and Ox_o, free dye concentrations in the lumen or outside the lumen, respectively; Ox_{bi} and Ox_{bo}, bound dye concentration onto the internal or external, respectively, vesicle leaflets.

The free form of the permeant lipophilic anion oxonol VI is expected to accumulate in the vesicle lumen at thermodynamic equilibrium with positive inside membrane potential (E_m):

$$E_m = (RT/F)\ln(Ox_l/Ox_o) \tag{A1}$$

The membrane potential E_m can be calculated from the ratio Ox_{bl}/Ox_{bo} of the dye bound onto internal and external membrane leaflets, measured as $2Rt + 1$ (see text), in place of the ratio of the free dye Ox_l/Ox_o if 1) the relation bound versus free dye concentrations is linear (Ox_o and $Ox_i \ll K_d$ of membrane sites) and 2) there is no significant depletion of the free external concentration ($Ox_o \approx Ox_t$). The E_m value calculated in this way (E_{probe1}) was twofold lower than that expected (see Fig. 6 and text), because the two above conditions were not totally fulfilled. The aim of the treatment below is to analyze the relation between Ox_{bl}/Ox_{bo} and Ox_l/Ox_o as a function of F_w, Ft_{Em}, and Ft_0, measured in each record (see Fig. 1), to correct the observed Ox_{bl}/Ox_{bo} (i.e., $2Rt + 1$) for partial depletion of the free dye or for partial saturation of the internal leaflet. In the following, the fluorescence intensities F_w, Ft_{Em}, and Ft_0 are the values after correction for the intrinsic fluorescence of the buffer and successive dilutions (see Fig. 1).

Correction for the depletion of the free form of oxonol VI due to its binding onto membrane vesicles

The total internal volume of vesicles was lower than 0.02% of the external one; the proportion of the free dye accumulated in the vesicle lumen remained negligible, even at the higher E_m (125 mV). Therefore, the depletion of the free dye arose from its binding onto membrane vesicles. This can be accounted for from the values of F_w, Ft_{Em}, and Ft_0 and the relative (bound/free) fluorescence yield of the dye (Φ_r), as follows.

The initial concentration of free external oxonol Ox_o (Ox_t), corresponding to the fluorescence F_w, decreases down to Ox'_o (corresponding to F'_w) upon membrane vesicles addition at zero E_m, and down to Ox''_o (corresponding to F''_w) upon E_m generation. Accordingly, Ox_{bo} diminishes down to Ox'_{bo} (corresponding to $F'_0/2$) and Ox''_{bo} (corresponding to $F''_0/2$). As the maximal value of Ox_o ($Ox_t = 0.05$ μM) is ~100-fold lower than the dissociation constant of membrane sites, Ox_{bo} is to decrease linearly with Ox_o, and thus F_0 with F_w:

$$F'_0/F'_w = F''_0/F''_w \tag{A2}$$

Therefore, the fluorescence of bound and free dye is actually distributed after vesicle addition according to

$$F_w + F_0 = F'_w + F'_0 = Ft_0 \tag{A3}$$

and similarly, considering the fluorescence of total bound dye ($Ox_{bo} + Ox_{bl}$) onto both membrane leaflets ($F = F_0 + \Delta F$; see Fig. 1) after E_m generation:

$$Ft_{Em} = F''_w + F'' = F''_w + F''_0 + \Delta F'' \tag{A4}$$

The fraction of free oxonol is given by $(Fm_{lip} - F'_0)/Fm_{lip}$ after vesicles addition and by $(Fm_{lip} - F'')/Fm_{lip}$ after E_m generation, where Fm_{lip} is the maximal fluorescence of the dye totally bound onto the membrane (Fig. 4 and Table 1). Thus, F'_w and F''_w are given by

$$F'_w = F_w(Fm_{lip} - F'_0)/Fm_{lip} \tag{A5}$$

$$F''_w = F_w(Fm_{lip} - F'')/Fm_{lip} \tag{A6}$$

Denoting Φ_{lip} and Φ_w the fluorescence efficiency of bound and free oxonol, respectively, the following set of equations is experimentally important:

$$Fm_{lip} = \Phi_{lip}Ox_t \text{ and } F_w = \Phi_w Ox_t, \text{ giving } Fm_{lip} = \Phi_r F_w \tag{A7}$$

Indeed, the ratio of the fluorescence efficiencies $\Phi_r = \Phi_{lip}/\Phi_w$, determined by titrating the dye with vesicles (Fig. 4), is an intrinsic and reproducible characteristic of the dye-membrane interaction in the conditions used for the assay (see Table 1). On the other hand, Φ_{lip} and Φ_w, and therefore Fm_{lip} and F_w, may vary throughout the experimentation because they depend on the set-up of the spectrofluorometer (they are expressed in arbitrary units). Fortunately, the current value of F_w can be easily measured at the beginning of each record (see Fig. 1), and thus used to estimate Fm_{lip} ($\Phi_r F_w$). Replacing this expression of Fm_{lip} in Eqs. A5 and A6 gives

$$F'_w = (\Phi_r F_w - F'_0)/\Phi_r \text{ and } F''_w = (\Phi_r F_w - F'')/\Phi_r \tag{A8}$$

F'_0 can be explicitly taken from Eqs. A3 and A9:

$$F'_0 = \Phi_r(Ft_0 - F_w)/(\Phi_r - 1), \tag{A9}$$

giving in turn $F_{w'}$ from Eq. A9:

$$F'_w = (F_w\Phi_r - Ft_0)/(\Phi_r - 1) \tag{A10}$$

F''_w can be similarly taken from Eqs. A4 and A10:

$$F''_w = (\Phi_r F_w - Ft_{Em})/(\Phi_r - 1) \tag{A11}$$

These expressions of F'_0, F'_w, F''_w allowed to calculate F''_0 from Eq. A2:

$$F''_0 = \Phi_r((\Phi_r F_w - Ft_{Em})(Ft_0 - F_w))/((\Phi_r F_w - Ft_0)(\Phi_r - 1)), \tag{A12}$$

and F'' can be calculated from Eqs. A4 and A10:

$$F'' = \Phi_r(Ft_{Em} - F_w)/(\Phi_r - 1), \tag{A13}$$

giving $\Delta F''$ from Eq. A4:

$$\Delta F'' = \Phi_r F_w(Ft_{Em} - Ft_0)/(\Phi_r F_w - Ft_0) \tag{A14}$$

Finally, Eqs. A12 and A14 allow us to calculate the value of $Rt''_i = \Delta F''/F_{o''}$, accounting for the depletion of the free form of the dye:

$$Rt''_i = F_w((Ft_{Em} - Ft_0)(\Phi_r - 1))/((\Phi_r F_w - Ft_{Em})(Ft_0 - F_w)) \tag{A15}$$

Equation A15 allows us to measure the actual accumulation ratio Ox_{bl}/Ox_{bo} ($2Rt_i + 1$), following E_m generation, from the value of F_w, Ft_{Em}, and Ft_0 measured in each record. Provided that Ox_{bl} remains actually linear with Ox_l, E_m (E_{probe2}) can be calculated from Eq. A1:

$$E_{probe2} = (RT/F)\ln(2Rt''_i + 1) \tag{A16}$$

Correction for the saturation of the internal membrane leaflet by oxonol VI at high E_m

Oxonol binds onto membrane vesicles according to a mass action law (Fig. 5):

$$Ox_b = N\,Lip\,Ox/(K_d + Ox) \tag{A17}$$

where N, Lip, and K_d are the number of sites per unit of phospholipid concentration, the phospholipid concentration, and the dissociation constant, respectively. From the K_d and Oxt values (6 μM and 0.05 μM, respectively), Ox_{bo} is expected to remain linear with Ox_o ($Ox_{bo} = N\,Lip\,Ox_o/K_d$), because the latter decreases upon positive E_m generation. By contrast, Ox_l is expected to become close to K_d at high E_m and thus Ox_{bl} to become nonlinear with Ox_l. Developing the binding equation of oxonol onto both membrane leaflets allows us to express Ox_l/Ox_o, used to calculate E_m (Eq. A1), as a function of Ox_{bl}/Ox_{bo} ($2Rt''_i + 1$):

$$\begin{aligned} Ox_l/Ox_o &= (Ox_{bl}/Ox_{bo})N\,Lip/(N\,Lip - 2Ox_{bl}) \\ &= (2Rt''_i + 1)N\,Lip/(N\,Lip - 2Ox_{bl}) \end{aligned} \tag{A18}$$

The value of N (Table 1) has been determined from the titrations in Figs. 4 and 5. As the fraction of bound dye is given by F''/Fm_{lip}, and from Eq. A7:

$$Ox_{bo} + Ox_{bl} = Oxt\,F''/Fm_{lip} = Oxt\,F''/(\Phi_r F_w) \tag{A19}$$

Introducing F'' from Eq. A13, gives

$$Ox_{bo} + Ox_{bl} = Oxt(Ft_{Em} - F_w)/(F_w(\Phi_r - 1)), \tag{A20}$$

as Ox_{bl}/Ox_{bo} is given by ($2Rt''_i + 1$), when the free probe depletion is accounted for:

$$Ox_{bl} = Oxt(Rt''_i + 0.5)(Ft_{Em} - F_w)/((Rt''_i + 1)((\Phi_r - 1)F_w)) \tag{A21}$$

Introducing Eq. A21 in Eq. A18 permits us to calculate E_m (E_{probe3}) from Eq. A1 as

$$\begin{aligned} (RT/F)\ln[\{2Rt''_i + 1\}/\{1 - (Oxt(2Rt''_i + 1) \\ \cdot (Ft_{Em} - F_w))/(N\,Lip\,F_w(Rt''_i + 1)(\Phi_r - 1))\}] \end{aligned} \tag{A22}$$

In summary, the parameters Φ_r and N, required in the equations above and which characterize the membrane dye interaction, are first determined by titrations. Thereafter, F_w and Ft_0 are measured at the beginning of each assay, and introduced in Eq. A15 to calculate $Rt''_i f$(time) from $Ft_{Em} f$(time), accounting for the free dye depletion. Finally, $Rt''_i f$(time) is used to calculate $E_m f$(time) using Eq. A22, accounting in addition for partial saturation of the internal membrane leaflet of the vesicles.

Helpful discussions during this work and critical reading of our manuscript by Prof. C. Grignon are gratefully acknowledged. We also thank Prof. J. Guern (Institut des Sciences Végétales, CNRS, Gif-sur-Yvette, France) and Dr. F. Guillain (Département de Biologie Cellulaire et Moléculaire, C.E.A. de Saclay, Gif-sur Yvette, France) for interest and valuable comments. We are also indebted to Dr. J. Widmar for his kind revision of the manuscript.

Dr. P. Pouliquin was the recipient of a grant from the Ministère de la Recherche et de l'Education.

REFERENCES

Ackers, G. K. 1967. A new calibration procedure for gel filtration columns. *J. Biol. Chem.* 242:3237–3238.

Apell, H. J., and B. Bersch. 1987. Oxonol VI as an optical indicator for membrane potential in lipids vesicles. *Biochim. Biophys. Acta.* 903: 480–494.

Bammel, B. P., J. A. Brand, R. B. Simmons, D. Evans, and J. C. Smith. 1987. The interaction of potential-sensitive molecular probes with dimyristoylphophatidylcholine vesicles investigated by ^{31}P-NMR and electron microscopy. *Biochim. Biophys. Acta.* 896:136–152.

Bashford, C. L., B. Chance, and R. C. Prince. 1979. Oxonol dyes as monitors of membrane potential: their behavior in photosynthetic bacteria. *Biochim. Biophys. Acta.* 545:46–47.

Beyer, C. F., C. G. Lyman, and W. A. Gibbons. 1972. Interaction of the fluorescent probe 2p-toluidinylnaphthalene-6-sulfonate with peptides: structural requirements for binding and fluorescence enhancement. *Biochemistry.* 11:4920–4925.

Clarke, R. J., and H. J. Apell. 1989. A stopped-flow kinetic study of the interaction of potential-sensitive oxonol dyes with lipid vesicles. *Biophys. Chem.* 34:225–237.

Delhon, P., A. Gojon, P. Tillard, and L. Passama. 1995. Diurnal regulation of NO_3^- uptake in soybean plants. I. Changes in NO_3^- influx, efflux, and N utilization in the plant during the day/night cycle. *J. Exp. Bot.* 46:1585–1594.

De Michelis, M. I., and R. M. Spanswick. 1986. H^+-pumping driven by the vanadate-sensitive ATPase in membrane vesicles from corn roots. *Plant Physiol.* 81:542–547.

Devaux, P. H. 1981. Solubility of intrinsic membrane proteins in phospholipid bilayers. *In* Membranes and Intercellular Communication. R. Balian, M. Chabre, and P. H. Devaux, editors. North-Holland, Amsterdam. 93–115.

Galtier, N., A. Belver, R. Gibrat, J.-P. Grouzis, J. Rigaud, and C. Grignon. 1988. Preparation of corn root plasmalemma with low Mg-ATPase latency and high electrogenic H^+-pumping activity after phase partitioning. *Plant Physiol.* 87:491–497.

Gibrat, R., and C. Grignon. 1983. A procedure for estimating the surface potential of charged or neutral membranes with 8-anilino-1-naphthalenesulphonate probe: adequacy of the Gouy-Chapman model. *Biochim. Biophys. Acta.* 736:196–202.

Gradmann, D., U.-P. Hansen, W. S. Long, C. L. Slayman, and J. Warncke. 1978. Current-voltage relationships for plasma membrane and its principal electrogenic pump in *Neurospora crassa.* I. Steady-state conditions. *J. Membr. Biol.* 39:333–367.

Gronewald, J. W., W. Abou-Khalil, E. J. Weber, and J. B. Hanson. 1982. Lipid composition of a plasma membrane enriched fraction of maize roots. *Phytochemistry.* 21:859–862.

Grouzis, J.-P., P. Pouliquin, J. Rigaud, C. Grignon, and R. Gibrat. 1997. *In vitro* study of passive nitrate transport by native and reconstituted plasma membrane vesicles from corn root cells. *Biochim. Biophys. Acta.* 1325:329–342.

Gutknecht, J., and A. Walter. 1981. Hydrofluoric and nitric acid transport through lipid bilayer membranes. *Biochim. Biophys. Acta.* 644:153–156.

Hedrich, R., and I. Marten. 1993. Malate-induced feedback regulation of plasma membrane anion channels could provide a CO_2 sensor to guard cells. *EMBO J.* 12:897–901.

Hille, B. 1992. Ionic Channels of Excitable Membranes. Sinauer Associates, Sunderland, MA.

Huang, J. W., D. L. Grunes, and L. V. Kochian. 1994. Voltage-dependent Ca^{2+} influx into right-side-out plasma membrane vesicles isolated from wheat roots: characterization of a putative Ca^{2+} channel. *Proc. Natl. Acad. Sci. U.S.A.* 91:3473–3477.

Kaestner, K. H., and H. Sze. 1987. Potential dependent anion transport in tonoplast vesicles from oat roots. *Plant Physiol.* 83:483–489.

Lakshminarayanaiah, N. 1984. Equations of Membrane Biophysics. Academic Press, London.

Läuger, P. 1980. Kinetic properties of ion carriers and channels. *J. Membr. Biol.* 57:163–178.

Marshall, J., A. Corzo, R. A. Leigh, and D. Sanders. 1994. Membrane potential dependent calcium transport in right-side-out plasma membrane vesicles from *Zea mays* L. roots. *Plant J.* 5:683–694.

Mueller, P., T. F. Chien, and B. Rudy. 1983. Formation and properties of cell-size lipid bilayer vesicles. *Biophys. J.* 44:375–381.

Ohki, S. 1981. Membrane potential, surface potential and ionic permeabilities. *Physiol. Chem. Phys.* 13:195–210.

Ollivon, M., A. Walter, and R. Blumenthal. 1986. Sizing and separation of liposomes, biological vesicles, and viruses by high-performance liquid chromatography. *Anal. Biochem.* 152:262–274.

Philippot, J., S. Mutaftschiev, and J. P. Liautard. 1983. A very mild method allowing the encapsulation of very high amounts of macromolecules into very large (1000 nm) unilamellar liposomes. *Biochim. Biophys. Acta.* 734:137–143.

Reynolds, J. A., Y. Nozaki, and C. Tanford. 1983. Gel-exclusion chromatography on S1000 Sephacryl: application to phospholipid vesicles. *Anal. Biochem.* 130:471–474.

Ros, R., C. Romieu, R. Gibrat, and C. Grignon. 1995. The plant inorganic pyrophosphatase does not transport K^+ in vacuole membrane vesicles multilabeled with fluorescent probes for H^+, K^+, and membrane potential. *J. Biol. Chem.* 270:4368–4374.

Rossignol, M., P. Thomas, and C. Grignon. 1982. Proton permeability of liposomes from natural phospholipid mixtures. *Biochim. Biophys. Acta.* 684:195–199.

Rottenberg, H. 1989. Proton electrochemical potential gradients in vesicles, organelles, and prokaryotic cells. *Methods Enzymol.* 172:63–84.

Ryan, P. R., M. Skerrett, G. P. Findlay, E. Delhaize, and S. D. Tyerman. 1997. Aluminium activates an anion channel in the apical cells of wheat roots. *Proc. Natl. Acad. Sci. U.S.A.* 94:6547–6552.

Sanders, D., and C. L. Slayman. 1989. Transport at the plasma membrane of plant cells: a review. *In* Plant Membrane Transport: The Current Position. J. Dainty, M. I. De Michelis, E. Marrè, F. Rasi-Caldogno, editors. Elsevier/North Holland, Amsterdam. 3–11.

Schachtman, D. P., J. I. Schroeder, W. J. Lucas, J. A. Anderson, and R. F. Gaber. 1992. Expression of an inward-rectifying potassium channel by the *Arabidopsis KAT1* cDNA. *Science.* 258:1654–1658.

Schachtman, D. P., S. D. Tyerman, and B. R. Terry. 1991. The K^+/Na^+ selectivity of a cation channel in the plasma membrane of root cells does not differ in salt-tolerant and salt-sensitive wheat species. *Plant Physiol.* 97:598–605.

Schaffner, W., and C. Weissmann. 1973. A rapid, sensitive and specific method for the determination of protein in dilute solution. *Anal. Biochem.* 56:502–514.

Schlieper, P., P. K. Medda, and R. Kaufmann. 1981. Drug-induced zeta potential changes in liposomes studied by laser doppler spectroscopy. *Biochim. Biophys. Acta.* 644:273–283.

Schmidt, C., and J. I. Schroeder. 1994. Anion selectivity of slow anion channel in the plasma membrane of guard cells. *Plant Physiol.* 106: 383–391.

Serrano, R. 1989. Structure and function of plasma membrane ATPase. *Annu. Rev. Plant Physiol. Plant Mol. Biol.* 40:61–94.

Simon-Plas, F., K. Venema, J.-P. Grouzis, R. Gibrat, and C. Grignon. 1991. Spontaneous insertion of plant plasma membrane (H^+)ATPase into a preformed bilayer. *J. Membr. Biol.* 120:51–58.

Stein, W. D. 1986. Transport and Diffusion Across Cell Membranes. Academic Press, Orlando, FL.

Sukhorukov, V. L., C. S. Djuzenova, W. M. Arnold, and U. Zimmermann. 1994. DNA, protein and plasma membrane incorporation by arrested mammalian cells. *J. Membr. Biol.* 142:77–92.

Teissie, J., and T. Y. Tsong. 1981. Electric field induced transient pores in phospholipid bilayer vesicles. *Biochemistry.* 20:1548–1554.

Thibaud, J.-B., A. Soler, and C. Grignon. 1986. H^+ and K^+ electrogenic exchange in corn roots. *Plant Physiol.* 81:847–853.

Venema, K., R. Gibrat, J.-P. Grouzis, and C. Grignon. 1993. Quantitative measurement of cationic fluxes, selectivity and membrane potential using liposomes multilabelled with fluorescent probes. *Biochim. Biophys. Acta.* 1146:87–96.

Verhoven, B., R. A. Schlegel, and P. Williamson. 1992. Rapid loss and restoration of lipid asymmetry by different pathways in resealed erythrocytes ghosts. *Biochim. Biophys. Acta.* 1104:15–23.

Very, A.-A., F. Gaymard, C. Bosseux, H. Sentenac, and J.-B. Thibaud. 1995. Expression of a cloned plant K^+ channel in *Xenopus* oocytes: analysis of macroscopic currents. *Plant J.* 7:321–332.

Zhen, R. G., S. J. Smith, and A. J. Miller. 1992. A comparison of nitrate selective microelectrodes made with different nitrate sensors and the measurement of intracellular nitrate activities in cells of excised barley roots. *J. Exp. Bot.* 247:131–138.